

Structural health rating (SHR)-oriented 3D multi-scale finite element modeling and analysis of Stonecutters Bridge

X.F. Li^{1,2}, Y.Q. Ni^{*1}, K.Y. Wong³ and K.W.Y. Chan⁴

¹*Department of Civil and Environmental Engineering, The Hong Kong Polytechnic University, Kowloon, Hong Kong*

²*Institute of Road and Bridge Engineering, Dalian Maritime University, Dalian, China*

³*Formerly Bridges and Structures Division, Highways Department, The Hong Kong Special Administrative Region, Hong Kong*

⁴*Bridges and Structures Division, Highways Department, The Hong Kong Special Administrative Region, Hong Kong*

(Received February 10, 2014, Revised May 5, 2014, Accepted May 27, 2014)

Abstract. The Stonecutters Bridge (SCB) in Hong Kong is the third-longest cable-stayed bridge in the world with a main span stretching 1,018 m between two 298 m high single-leg tapering composite towers. A Wind and Structural Health Monitoring System (WASHMS) is being implemented on SCB by the Highways Department of The Hong Kong SAR Government, and the SCB-WASHMS is composed of more than 1,300 sensors in 15 types. In order to establish a linkage between structural health monitoring and maintenance management, a Structural Health Rating System (SHRS) with relevant rating tools and indices is devised. On the basis of a 3D space frame finite element model (FEM) of SCB and model updating, this paper presents the development of an SHR-oriented 3D multi-scale FEM for the purpose of load-resistance analysis and damage evaluation in structural element level, including modeling, refinement and validation of the multi-scale FEM. The refined 3D structural segments at deck and towers are established in critical segment positions corresponding to maximum cable forces. The components in the critical segment region are modeled as a full 3D FEM and fitted into the 3D space frame FEM. The boundary conditions between beam and shell elements are performed conforming to equivalent stiffness, effective mass and compatibility of deformation. The 3D multi-scale FEM is verified by the in-situ measured dynamic characteristics and static response. A good agreement between the FEM and measurement results indicates that the 3D multi-scale FEM is precise and efficient for WASHMS and SHRS of SCB. In addition, stress distribution and concentration of the critical segments in the 3D multi-scale FEM under temperature loads, static wind loads and equivalent seismic loads are investigated. Stress concentration elements under equivalent seismic loads exist in the anchor zone in steel/concrete beam and the anchor plate edge in steel anchor box of the towers.

Keywords: Structural health rating (SHR) system; Stonecutters Bridge; cable-stayed bridge; multi-scale finite element model (FEM)

*Corresponding author, Professor, E-mail: ceyqni@polyu.edu.hk

1. Introduction

With the rapid development of long-span bridges over the past two decades, implementation of structural health monitoring systems for important bridges has been increasingly accepted (Mufti 2002, Pine and Aktan 2002, Wong 2004, Ko and Ni 2005, Brownjohn 2007, Habel 2009, Ou and Li 2009, Ni *et al.* 2011, Yun *et al.* 2011, Phares *et al.* 2013, Seo *et al.* 2013). Diagnostic and prognostic analyses of the structural and durability performance of cable-supported bridges under in-service conditions are an essential strategy for planning and scheduling of inspection and maintenance activities. To fulfill this task, an accurate FEM of the bridge is desired to perform effective assessment of the required structural and durability performance. There have been a number of studies on the finite element modeling of cable-supported bridges to facilitate static and dynamic analyses (Wilson and Gravelle 1991, Brownjohn *et al.* 1999, Chang *et al.* 2001, Freire *et al.* 2006, Wei *et al.* 2012, Hassan 2013). Among many works, the FEM updating of large-scale bridges in reliance on ambient vibration testing results and modal identification techniques has been widely investigated in recent years (Brownjohn and Xia 2000, Cunha *et al.* 2001, Zhang *et al.* 2001, Daniell and Macdonald 2005, Ren *et al.* 2005, Kim *et al.* 2013).

Simplified spine beam FEMs of equivalent sectional properties to the actual bridge components have been widely adopted in modeling of cable-supported bridges (Zhang *et al.* 2001, Caicedo *et al.* 2003, Gentile and Gennari-Santori 2006, Hua *et al.* 2009, Talebinejad *et al.* 2011). This kind of FEMs is effective to evaluate the global dynamic characteristics and global structural behavior of a complex bridge with high computational efficiency. However, critical local damage under static and dynamic loading cannot be estimated directly through stress and strain nephogram in the spine beam FEMs. On the other hand, it is obviously impossible to elaborately model and analyze the global and local behavior of structural response and damage in a unified spatial scale, because even the simple task with ordinary load case becomes extremely difficult to execute with the existing computing power in full 3D FEMs. As a result, it is highly desirable to develop a numerical approach in multiple spatial scales for modeling and predicting dynamic response and local damage of large-scale structures such as long-span bridges. Attempts to develop such multi-scale FEMs are an effective approach for long-span bridges. Accurate evaluation of the effect of possible damage in critical components on the global dynamic characteristics of a bridge structure is of critical importance in developing a robust structural damage identification scheme particularly for a long-span bridge. The strategy for finite element modeling of a long-span cable-stayed bridge for multi-scale numerical analysis has been studied (Ding *et al.* 2010). A multi-scale model of the suspension Tsing Ma Bridge has been developed for the purpose of multi-scale numerical analysis (Li *et al.* 2007). By referring to a 3-dimensional FEM, a procedure for multi-scale analysis of dynamic response and structural damage of the suspension Runyang Bridge has been proposed (Wang *et al.* 2010).

The cable-stayed SCB with a main span of 1,018 m is being instrumented with a sophisticated SHM system, called Wind and Structural Health Monitoring System (WASHMS) (Wong and Ni 2009, Ni *et al.* 2011). To facilitate condition-based maintenance and management of the bridge with the use of SHM data, a 3D bridge condition rating methodology in terms of criticality rating, vulnerability rating, and structural condition rating has been proposed (Ni and Wong 2012, Xia *et al.* 2013). It is formulated to carry out bridge condition rating in an updatable way based on the inspection and structural analysis results as well as cumulated SHM data. The criticality rating is to evaluate the inherent property such as mechanical characteristics (alternative load path, strength utilization factor, etc.) and failure mechanism of the bridge components. The vulnerability rating is

mainly to evaluate the fragility of the bridge components to the environment, which is the exposure degree, the likelihood of detection in superficial inspection, and the likely influence of damage at structural components on bridge integrity. The structural condition rating is to assess the current condition of bridge components based on the inspection results and maintenance records. An FEM of the bridge, which enables stress analysis in structural element level, is therefore desired to accomplish fundamental rating baseline establishment and load resistance strength evaluation. A simplified spine beam FEM is apparently incapable of stress analysis in structural element level, while a full 3D FEM for SCB is very difficult, if not impossible, to accomplish the load-resistance analysis at both serviceability limit state and ultimate limit state by running the FEM on a common PC computer. In the present study, an SHR-oriented 3D multi-scale FEM which enable stress and ultimate load-resistance strength analysis in structural element level while having considerable computational efficiency will be developed for SCB and calibrated with field measurement data.

2. Multi-scale FE modeling

2.1 Strategies for multi-scale FE modeling

When an FEM model is formulated for a large-scale bridge with the purpose of damage-relevant simulation and analysis, it is usually required to meet the following requirements (Ko *et al.* 1999, Ko and Ni 2005): (a) the FEM should be accurate enough through comparisons of the computed and measured structural characteristics (modal parameters, influence line, etc.); (b) the stiffness contribution of all individual structural components is independently described in the model, so that the sensitivity of global and local modal properties to the material or geometric parameters of any structural component can be computed accurately; and (c) damage occurring in any structural component can be directly simulated in the FEM. Based on this concept, a precise three-dimensional FEM could incorporate where necessary local detailed models into the global and component models depending on the purpose of analysis to achieve multi-scale FE modeling as shown in Fig. 1. The following strategies have been introduced in the multi-scale FE modeling of SCB:

(1) The multi-scale FEM should represent the modal properties of the real bridge accurately so that the essential static and dynamic analysis results of the FEM are well correlated with the measurement data;

(2) The multi-scale modeling for the critical segments of the bridge should be precise enough so that it can provide considerably accurate calculation of both load-induced and distortion-induced stress distribution/damage under specific loadings;

(3) A reasonable mesh method for complex bridge components with a tradeoff between the modeling accuracy and computational efficiency should be executed to reduce the unnecessary computation time; and

(4) The systematic output results of multi-scale FE analysis in non-linear calculation, dynamic wind stability analysis and dynamic seismic destructive evaluation should be compatible with SHRS for the execution of WASHMS.

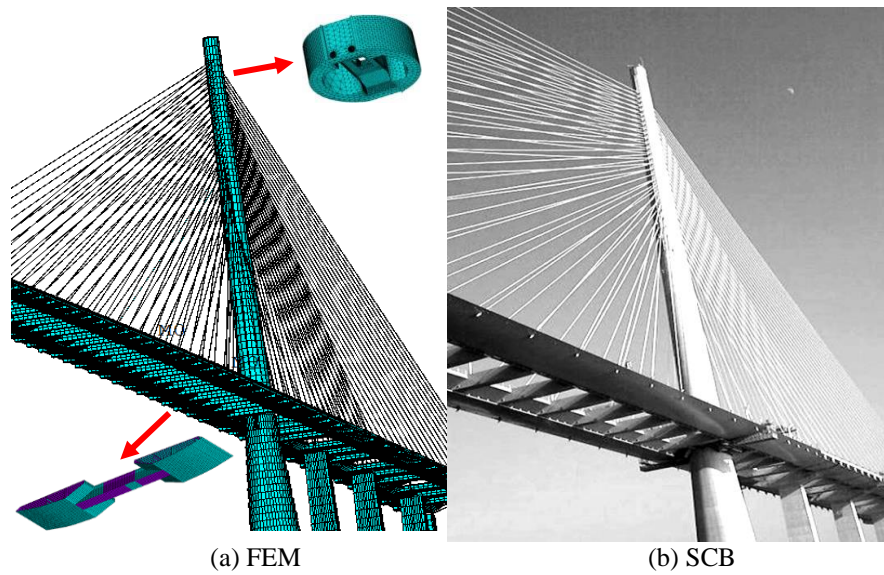


Fig. 1 Multi-scale FE modeling of SCB

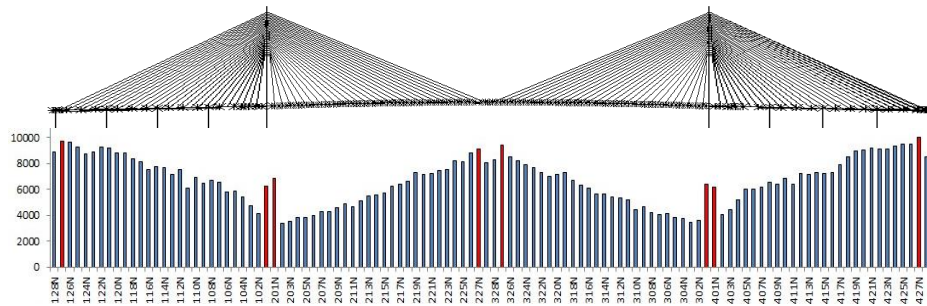
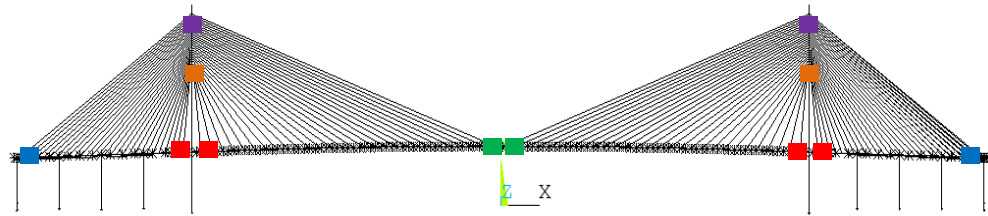


Fig. 2 Critical locations of stay cables in SCB

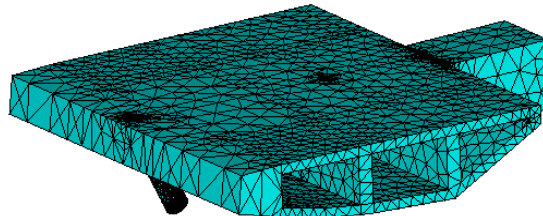
2.2 FE Modeling of Stonecutters Bridge

In the formulation of the multi-scale FEM, the critical segment positions of deck-stay connections and tower-stay connections in the cable plane are selected as the cables with highest force in respective side-span and central span. Fig. 2 shows the measurement-derived values of stay cable forces in SCB. The highest cable force critical locations in the diagonal members of the north outer-longitudinal deck are determined from the figure as: the cables No. N127, N227, N327, N427. Furthermore, four cables close to the two towers are also identified as critical locations owing to abrupt change of the cable force. According to the strategies for multi-scale FE modeling, five critical segments of SCB are identified and will be modeled spatially, as shown Fig. 3, which include: (a) concrete beam segment, (b) steel beam segment with web plate, (c) steel beam segment without web plate, (d) concrete tower segment with anchorage box, and (e) concrete tower segment without anchorage box.

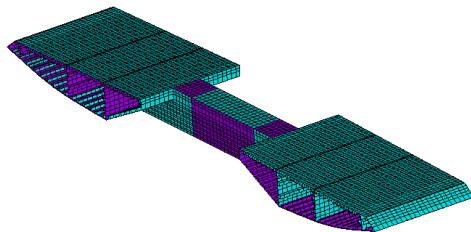


- FE Segment model 1: Concrete beam segment
- FE Segment model 2: Steel beam segment with web plate
- FE Segment model 3: Steel beam segment without web plate
- FE Segment model 4: Concrete tower segment with anchorage box
- FE Segment model 5: Concrete tower segment without anchorage box

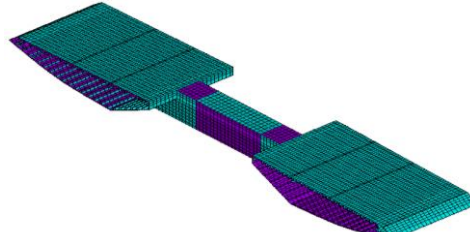
(a) Five critical segments of SCB



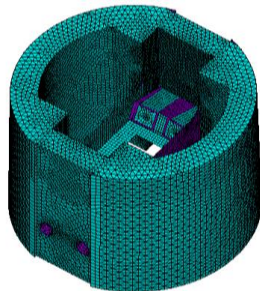
(b) FE segment model 1



(c) FE segment model 2



(d) FE segment model 3



(e) FE segment model 4



(f) FE segment model 5

Fig. 3 Multi-scale segment models of SCB

The concrete box-girder segment at the side spans of SCB is meshed into 98,000 concrete solid elements as shown in Fig. 4, including concrete anchorage section, steel anchor, cross concrete box-girder and concrete web.

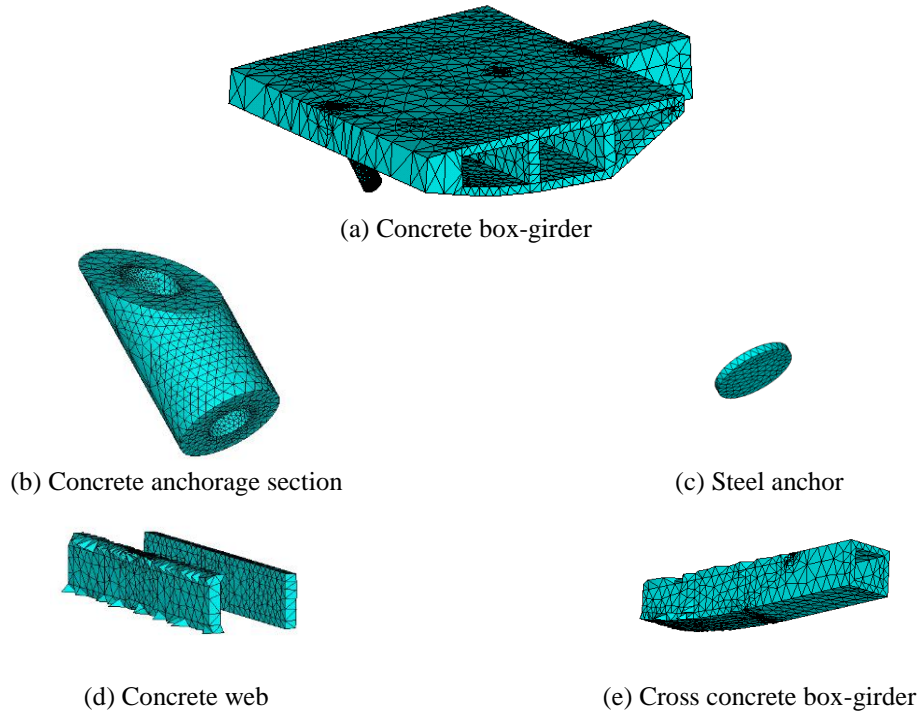


Fig. 4 FE segment model 1

The main span of the bridge is a twin-deck configuration consisting of two separated longitudinal box girders, which are linked by transverse beams. The steel beam segment with 140,000 shell elements is the second multi-scale FE model of the selected segment, as shown in Fig. 5, which includes stop plate, U-shape rib, bottom plate, cross box-girder, web plate, cross plate and beam anchorage. About 13,500 shell elements constitute the third model without web plate as illustrated in Fig. 6.

The fourth model is about the upper part of the towers as shown in Fig. 7, including steel skin, steel anchor box, concrete segment, cross plate, steel anchor and steel guide pipe, which are fully modeled by 160,000 solid elements and 40,000 shell elements. Fig. 8 shows the fifth multi-scale model of the concrete tower segment without anchor box owing to the design angle of cables.

2.3 Boundary conditions

The connection between the beam element and solid/shell element must be reasonably represented by boundary conditions, which should also conform to the equivalent stiffness, effective mass and compatibility of deformation. In the multi-scale model, the boundaries are modeled by a set of rigid link elements, which appropriately simulate the actual behavior between the beam element and 3D segment. In consideration of the stress concentration at the connection, each critical 3D segment, as shown in Fig. 9, is divided into one primary segment and two boundary segments. In line with the Saint-Venant's principle, the range of the boundary segments is optimized for computational efficiency.

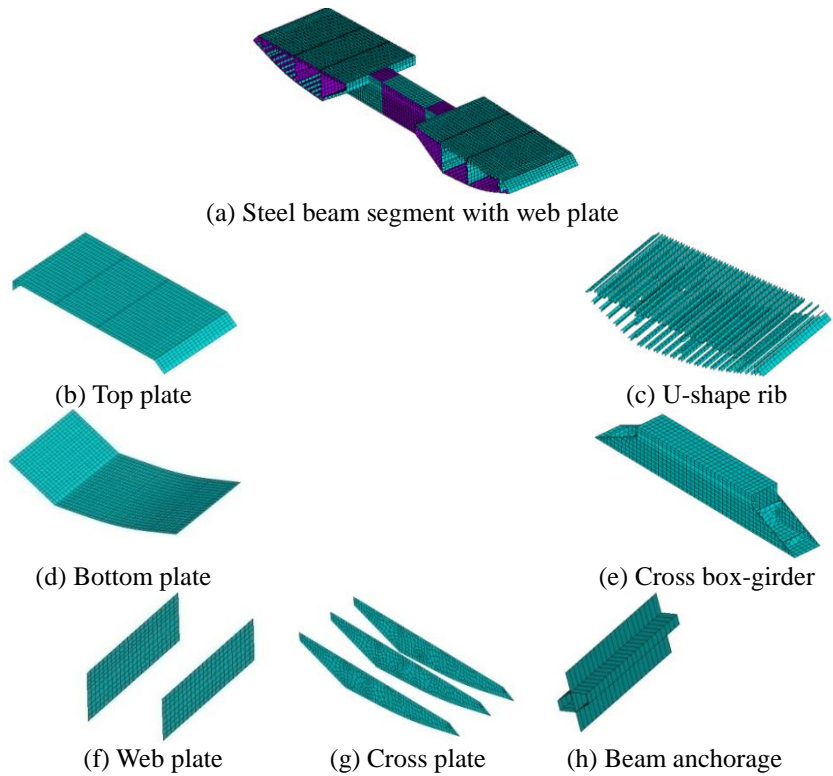


Fig. 5 FE segment model 2

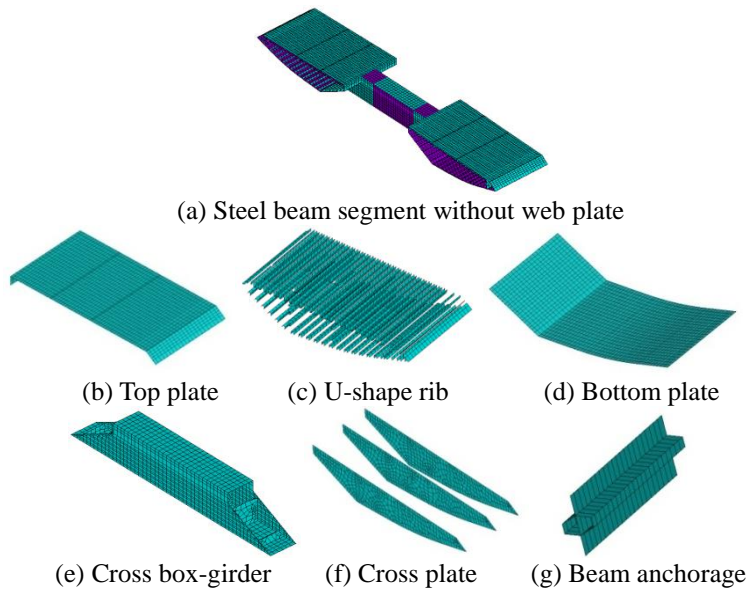


Fig. 6 FE segment model 3

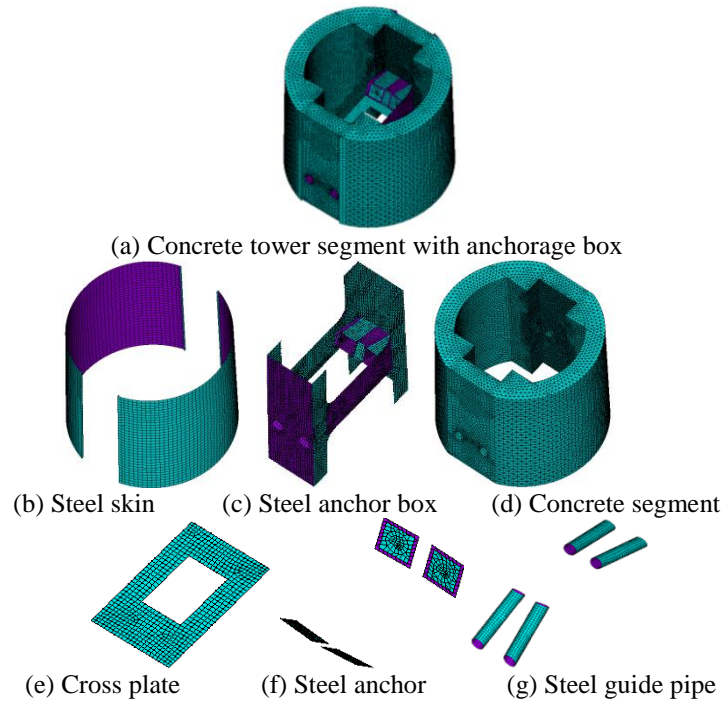


Fig. 7 FE segment model 4

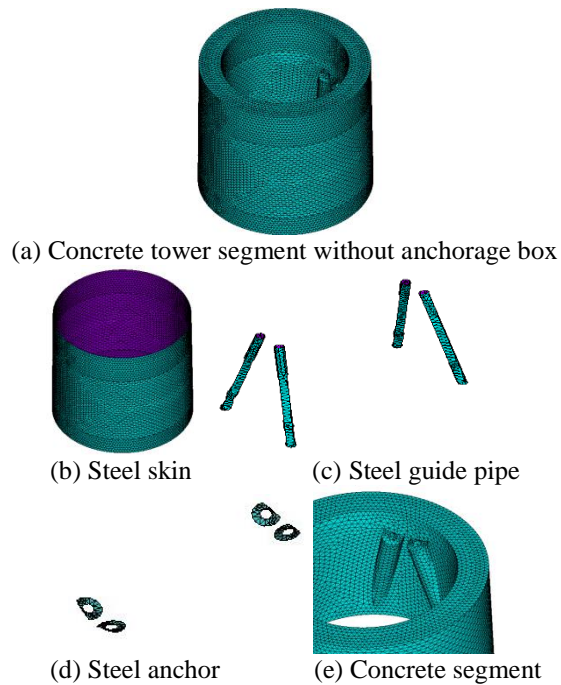


Fig. 8 FE segment model 5

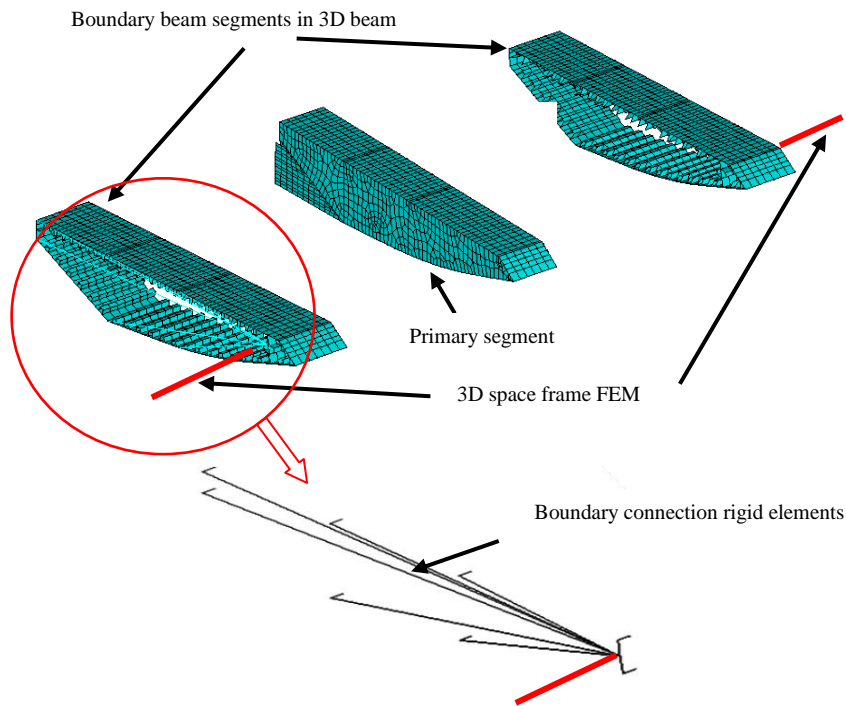


Fig. 9 Boundary conditions for connection in FE modelling of SCB

3. Static and dynamic model calibration

3.1 Static analysis

In the establishment of the multi-scale FEM, the coordinates of the bridge obtained from as-built drawings are taken as the target configuration. Therefore, the objective of the static calibration is to determine the initial cable forces which minimize the displacement response under dead load. After the static and dynamic model calibration for the multi-scale FEM of SCB with segment model 1, the difference of displacement in Y direction under dead load between calculation and as-built drawings is illustrated in Fig. 10. In the five multi-scale FE segment models, the maximum upward and downward displacements of the bridge deck fall below ± 3.92 cm. Cable force measurement using ambient vibration measurement was carried out by the Bridge Technical Advisory Section (BTAS) during 4-12 November 2009. The comparison of the cable forces between the multi-scale FE segment model 1 results and the measurement results is conducted with the relative differences being shown in Fig. 11. It is concluded that all the cable force differences between measurement and computation fall below $\pm 8\%$.

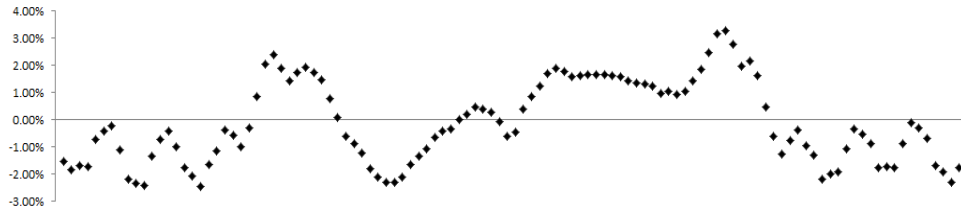


Fig. 10 Difference of displacement in Y direction between calculation and as-built drawings

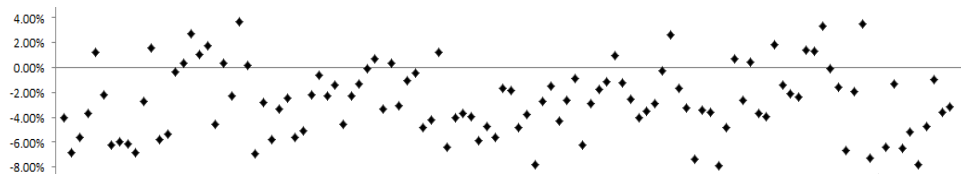


Fig. 11 Difference of cable forces between calculation and measurement

3.2 Comparison of modal frequencies

The frequency measurement of SCB after completion of the bridge deck was carried out by the Hong Kong SAR Highways Department. The computed modal frequencies from the five multi-scale FE segment models are compared with the measured results. The relative difference in modal frequencies is defined as

$$d = \frac{f^{Measure} - f^{FEM}}{f^{Measure}} \times 100\% \quad (1)$$

where f^{FEM} and $f^{Measure}$ are the computed and measured modal frequencies, respectively.

Table 1 compares the first 10 modal frequencies computed from the five multi-scale models with those measured by the Hong Kong SAR Highways Department. It can be seen that the results of the multi-scale FEM agree well with the measured ones. The relative differences fall below $\pm 4.37\%$.

3.3 Modal analysis

With considering the static stress under gravity load, the modal analysis was carried out in software ANSYS. The frequencies and modal properties of the first 10 modes are presented in Table 2. The mode shapes for the first 10 modes from the multi-scale FEM with segment model 4 are shown in Fig. 12. Dynamic interactions among vertical, lateral, torsional and longitudinal motions, among deck, cables and towers and among the main span and approach spans are observed.

Table 1 Comparison between measured and calculated modal frequencies

Mode No.	Measured (Hz)	Model 1		Model 2		Model 3		Model 4		Model 5	
		Freq.	Diff. (%)								
1st	0.1613	0.1593	1.26	0.1582	1.92	0.1577	2.23	0.1593	1.24	0.1593	1.24
2nd	0.2126	0.2120	0.27	0.2120	0.29	0.2117	0.42	0.2120	0.28	0.2120	0.28
3rd	0.2167	0.2179	-0.55	0.2179	-0.56	0.2179	-0.55	0.2176	-0.42	0.2177	-0.46
4th	0.2104	0.2193	-4.23	0.2192	-4.31	0.2191	-4.13	0.2190	-4.09	0.2191	-4.13
5th	0.2632	0.2580	1.98	0.2580	2.05	0.2575	2.17	0.2580	1.98	0.2580	1.98
6th	0.3268	0.3163	3.20	0.3162	3.37	0.3159	3.34	0.3162	3.24	0.3162	3.24
7th	0.3340	0.3337	0.09	0.3337	0.10	0.3322	0.54	0.3337	0.09	0.3336	0.12
8th	0.3952	0.3949	0.07	0.3908	1.19	0.3894	1.47	0.3949	0.08	0.3949	0.08
9th	0.4125	0.3958	4.04	0.3958	4.37	0.3951	4.22	0.3958	4.05	0.3957	4.07
10th	0.4586	0.4596	-0.21	0.4596	-0.24	0.4575	-0.24	0.4596	-0.22	0.4595	-0.20

Table 2 Modal analysis results from multi-scale FEM

Mode No.	Frequency (Hz)	Description of mode shapes
1st	0.1593	1st symmetric horizontal, girder
2nd	0.2120	1st asymmetric horizontal, tower
3rd	0.2176	1st symmetric horizontal, tower
4th	0.2190	1st symmetric vertical, girder
5th	0.2580	1st asymmetric horizontal, girder
6th	0.3162	Horizontal, piers and towers; Vertical, girder
7th	0.3337	2nd symmetric vertical, girder
8th	0.3949	1st asymmetric horizontal, girder
9th	0.3958	2nd asymmetric vertical, girder
10th	0.4596	Horizontal, back spans; Torsional, girder

Although a good agreement between the FEM and measured modal parameters was observed in the model verification, only the information of modal frequencies and mode shapes of the multi-scale FE model does not provide a sufficiently detailed indication of each mode participating in dynamic response. The modal participation factors and effective masses, computed from the mode shapes and mass matrix of the multi-scale FE model, indicate the relative importance of each mode when the structure is subjected to a ground motion excitation. Modes with relatively large effective masses contribute more to the dynamic response induced by the ground motion. In this study, the reference point is taken as the origin of the bridge coordinate system. The number of ground excitations considered is six: three translational and three rotational excitations. Table 3 shows the modal effective mass fractions of the first 30 modes of the multi-scale FEM with segment model 4. The columns (c), (d) and (e) in Table 3 show the modal effective mass fractions corresponding to the translational ground motion along x, y and z axes, respectively; while the columns (f), (g) and (h) are those corresponding to the ground rotation about x, y and z axes, respectively. The values in each column show the relative importance of a specific mode in terms

of response to the ground motion at a modal frequency. The total effective mass fraction at the bottom of each column gives the percentage of total rigid body mass that the above modes represent. It is found that the total effective mass fractions of the first 30 modes are relatively large except for translation y and rotational z . Therefore, 30 modes may be approximately sufficient for the dynamic response analysis of the global model.

Table 3 Modal effective mass fraction of multi-scale model with FE segment model 4

Mode No.	Frequency (Hz)	Modal effective mass fraction (%)					
		Translational degree of freedom			Rotational degree of freedom		
		x	y	z	x	y	z
(a)	(b)	(c)	(d)	(e)	(f)	(g)	(h)
1th	0.1593	0.00	0.00	14.03	16.40	0.00	0.00
2nd	0.2120	0.00	7.28	0.01	0.03	0.00	0.00
3rd	0.2176	0.00	0.00	1.11	4.51	15.07	0.00
4th	0.2190	0.00	0.00	13.54	52.41	1.51	0.00
5th	0.2580	1.71	0.00	0.00	0.00	0.00	0.26
6th	0.3162	77.11	0.00	0.00	0.00	0.00	2.17
7th	0.3337	0.00	2.56	0.00	0.00	0.00	0.00
8th	0.3949	0.00	0.00	0.01	0.00	0.07	0.00
9th	0.3958	0.13	0.00	0.00	0.00	0.00	0.44
10th	0.4596	0.00	0.96	0.00	0.00	0.00	0.00
11th	0.4736	0.00	0.00	0.73	0.59	0.00	0.00
12th	0.5270	0.14	0.00	0.00	0.00	0.00	0.22
13th	0.5764	0.00	0.00	20.03	8.55	24.66	0.00
14th	0.5887	0.00	0.33	0.00	0.00	0.00	0.00
15th	0.6113	0.00	0.00	9.13	3.90	32.67	0.00
16th	0.6438	0.00	0.00	0.00	0.00	0.15	0.00
17th	0.6479	0.01	0.52	0.00	0.00	0.00	0.00
18th	0.6525	0.00	0.00	17.45	9.32	0.29	0.00
19th	0.6627	0.39	0.00	0.00	0.00	0.00	0.11
20th	0.7312	0.00	0.00	0.00	0.00	3.62	0.00
21st	0.7420	0.00	0.51	0.00	0.00	0.00	0.00
22nd	0.7698	0.00	0.00	0.75	1.02	0.00	0.00
23rd	0.7839	0.00	0.00	0.25	0.33	0.00	0.00
24th	0.8116	1.00	0.00	0.00	0.00	0.00	0.01
25th	0.8703	0.18	0.29	0.00	0.00	0.00	0.29
26th	0.8745	1.64	0.00	0.00	0.00	0.00	2.71
27th	0.9083	0.01	3.67	0.00	0.00	0.00	0.00
28th	0.9278	0.00	0.00	0.00	0.00	0.13	0.00
29th	0.9604	0.00	0.03	0.00	0.00	0.00	1.62
30th	1.0138	0.00	0.95	0.00	0.00	0.00	0.01
Total effective mass fraction (%)		82.32	17.1	77.04	97.06	78.17	7.84

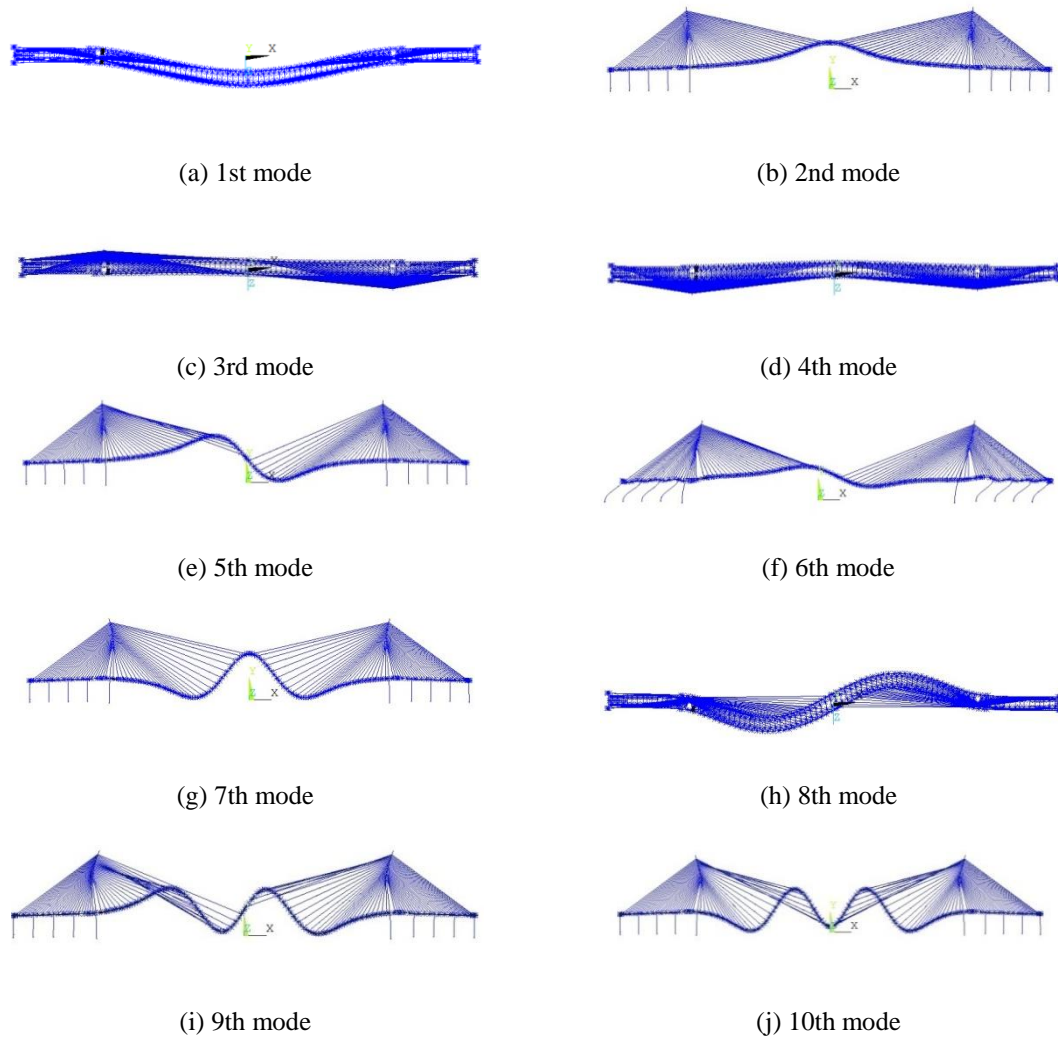


Fig. 12 Vibration modes obtained by multi-scale FEM with segment model 4

4. Multi-scale FE analysis

4.1 Temperature loads

This loading type is used to analyze the effect of dead loads plus temperature loads. Temperature loads refer to the structural effect of temperature variation in structural components and such variation is $\pm \Delta 28^{\circ}\text{C}$ for structural steel sections, $\pm \Delta 20^{\circ}\text{C}$ for cable steel sections, and $\pm \Delta 20^{\circ}\text{C}$ for structural concrete sections, respectively, as adopted in the design of SCB.

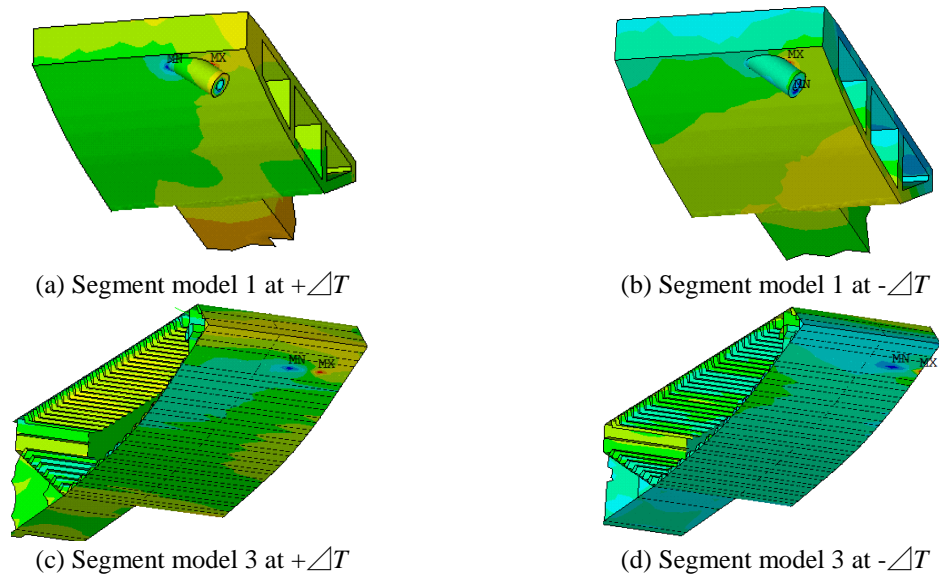


Fig. 13 Longitudinal stress distribution under temperature loads

Some of the typical details are illustrated in Fig. 13. The adverse local compressive stress is located at the bottom of the concrete beam in the side spans under $+\Delta T$ load case in Fig. 13(a), while it happens at the concrete anchor end under $-\Delta T$ load case in Fig. 13(b). The local tensile stress and compressive stress at the cable anchorage of steel beam, expressed as MX and MN respectively in stress nephogram, are higher in the case of $-\Delta T$ as shown in Fig. 13(d) than in the case of $+\Delta T$ as shown in Fig. 13(c) owing to greater tension of bridge cables under $-\Delta T$ load case.

4.2 Static wind loads

Wind loads refer to the equivalent wind forces at a wind speed of 50 m/s to 95 m/s distributed along the span-length of the bridge-deck and along the height of the towers as shown in Fig. 14. The values of mean wind speed and gust wind speed at bridge-deck level are 55 m/s (10-minute mean at 120-year return period) and 65 m/s (3-second gust at 120-year return period) respectively; whereas the gust wind speeds at towers and piers are 88 m/s (3-second gust at 120-year return period) and 82 m/s (3-second gust at 120-year return period) respectively.

The stress results of the steel beam in the main span under three wind load cases respectively, as given in Fig. 15, show small variation of longitudinal stress values in the region of segment model 3. Due to the difference of the three load cases, the highest local tensile stress and compressive stress are located at the anchorage zones in steel beam under load case 3 as shown in Fig.15(c).

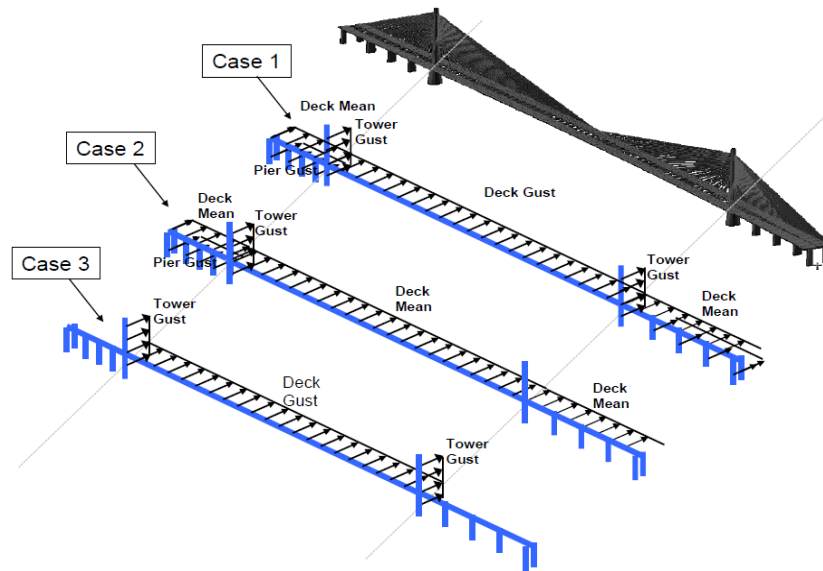


Fig. 14 Static wind load cases

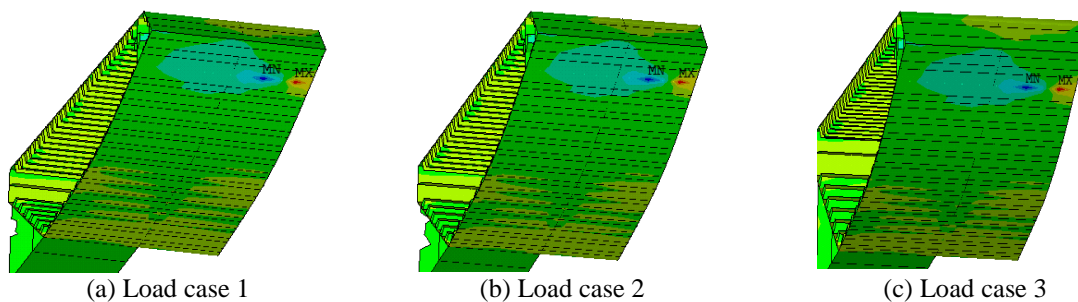


Fig. 15 Stress distribution under static wind loads

4.3 Equivalent seismic loads

Fig. 16 shows the equivalent seismic loads with three load cases, which refer to the equivalent horizontal forces acting on the bridge due to ground accelerations generated at foundations. The equivalent horizontal forces acting on the bridge, which are based on the assumption that the first few vibration modes of the deck and towers will be motivated by seismic loads.

Figs. 17(a) and 17(c) show the maximum longitudinal stress in the anchorage zone of segment model 3, and Fig. 17(b) gives the results of the maximum longitudinal tensile stress on the edge of the bridge deck segments under the seismic load. Figs. 17(d), (e) and (f) illustrate the region of vertical stress concentration at the welded joint intersection of the wall steel plate and anchor plate in steel anchor box of segment model 4. The most adverse effect is found in the steel anchor box under equivalent seismic load case 2 as shown in Fig. 17(e).

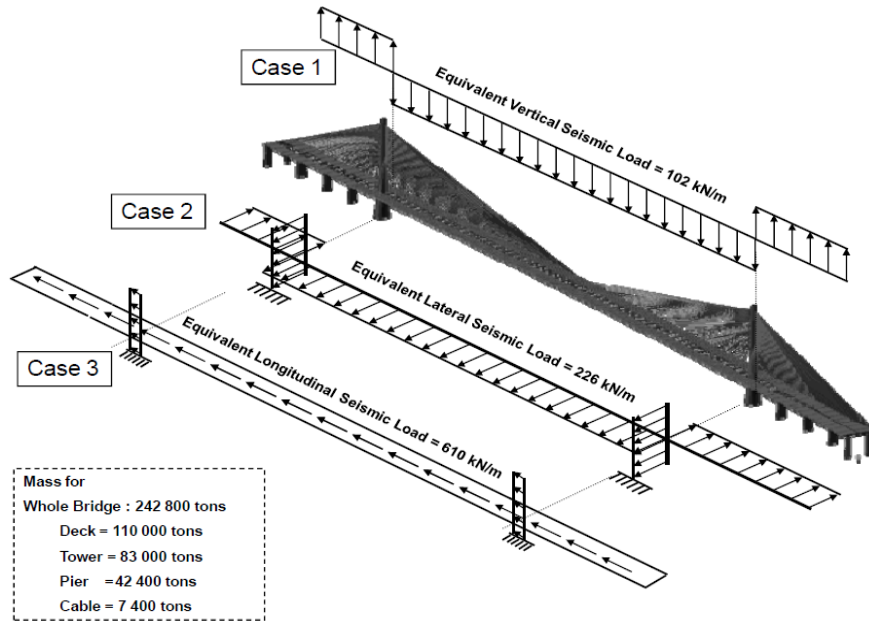


Fig. 16 Equivalent seismic load cases

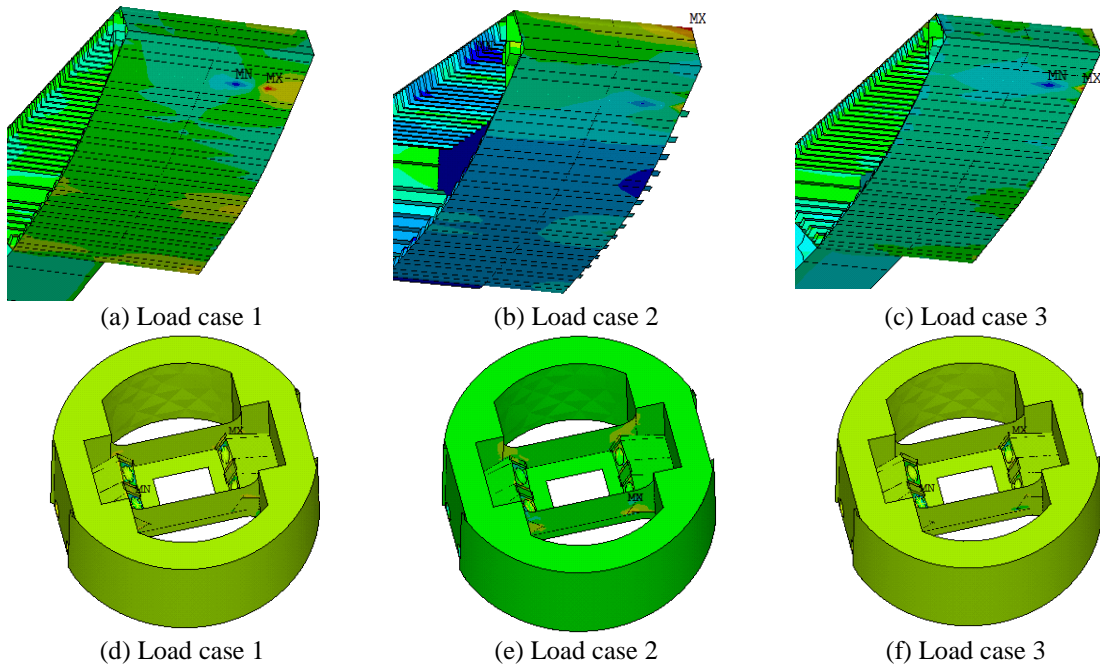


Fig. 17 Stress distribution under equivalent seismic loads

5. Conclusions

In this paper, the strategy and method for multi-scale FE modeling of a long-span cable-stayed bridge are presented for the purpose of multi-scale static and dynamic analyses and load resistance strength evaluation. Five multi-scale FE models including deck segments and tower segments in critical portions of SCB are formulated. Based on the results from the present study, the following conclusions can be drawn:

(1) Single-scale spine beam FE models fail to satisfy the requirements of local stress analysis on critical structural components of SCB, and full-scale 3D FE precise modeling is unsuitable for serviceability limit state and ultimate limit state evaluation of SCB under complicated load conditions owing to the limit of existing computing power. The proposed multi-scale FE modeling technique has high efficiency and accuracy on local component stress analysis, which has been validated by the in-situ experimental results. The multi-scale FEM is appropriate to accomplish fundamental rating baseline establishment and load resistance strength evaluation required for the SHRS;

(2) A key issue during the multi-scale analysis is to determine the length of the primary middle segment in a segment model. The results show that stress concentration near the two boundaries of the critical segment is very clear, and the influence length is about 1/3 of the critical segment in each of the two boundaries. Therefore, the stress located more than 1/3 critical segment to the boundary can be utilized to define the primary middle segment;

(3) The multi-scale FE modeling method for SCB is presented for a comprehensive representation of the global structure and critical components including concrete beam segment, steel beam segment and concrete tower segment with anchor box. The static and dynamic calibration of the model has been carried out, based on the measurement data of static configuration, cable forces and modal frequencies. A good agreement is observed between the computed results and the field measurements;

(4) The stress of the multi-scale FEM of SCB under unfavorable load cases is relatively low, but some results indicate that special attention should be given to the stress concentration elements under equivalent seismic loads, which exist in the anchor zone in steel/concrete beam and the anchor plate edge in steel anchor box of the towers.

Acknowledgments

The work described in this paper was supported by a grant from the Research Grants Council of the Hong Kong Special Administrative Region, China (Project No. PolyU5224/13E). The authors also wish to thank the Hong Kong SAR Government Highways Department for providing support to this research.

References

- Brownjohn, J.M.W. (2007), "Structural health monitoring of civil infrastructure", *Philos. T. R. Soc. A*, **365**(1851), 589-622.
- Brownjohn, J.M.W., Lee, J. and Cheong, B. (1999), "Dynamic performance of a curved cable-stayed bridge", *Eng. Struct.*, **21**(11), 1015-1027.

- Brownjohn, J.M.W. and Xia, P.Q. (2000), "Dynamic assessment of curved cable-stayed bridge by model updating", *J. Struct. Eng. - ASCE*, **126**(2), 252-260.
- Caicedo, J.M., Dyke, S.J., Moon, S.J., Bergman, L.A., Turan, G. and Hague, S. (2003), "Phase II benchmark control problem for seismic response of cable-stayed bridges", *J. Struct. Control*, **10**(3-4), 137-168.
- Chang, C.C., Chang, T.Y.P. and Zhang, Q.W. (2001), "Ambient vibration of long-span cable-stayed bridge", *J. Bridge Eng. - ASCE*, **6**(1), 46-53.
- Cunha, A., Caetano, E. and Delgado, R. (2001), "Dynamic tests on large cable-stayed bridge", *J. Bridge Eng. - ASCE*, **6**(1), 54-62.
- Daniell, W.E. and Macdonald, J.H.G. (2005), "Improved finite element modelling of a cable-stayed bridge through systematic manual tuning", *Eng. Struct.*, **29**(3), 358-371.
- Ding, Y.L., Li, A.Q., Du, D.S. and Liu, T. (2010), "Multi-scale damage analysis for a steel box girder of a long-span cable-stayed bridge", *Struct. Infrastruct. E.*, **6**(6), 725-739.
- Freire, A.M.S., Negro, J.H.O. and Lopes, A.V. (2006), "Geometrical nonlinearities on the static analysis of highly flexible steel cable-stayed bridges", *Comput. Struct.*, **84**(31-32), 2128-2140.
- Gentile, C. and Gennari-Santori, A. (2006), "Dynamic testing and modeling of a 30-years' old cable-stayed bridge", *Struct. Eng. Int.*, **16**(1), 39-43.
- Habel, W.R. (2009), "Structural health monitoring research in Europe: trends and applications", in: *Structural Health Monitoring of Civil Infrastructure Systems*, (Eds., V.M., Karbhari and F., Ansari), Wood head Publishing, Cambridge, UK.
- Hassan, M.M. (2013), "Optimization of stayed cables in cable-stayed bridges using finite element, genetic algorithm, and B-spline combined technique", *Eng. Struct.*, **49**, 643-654.
- Hua, X.G., Ni, Y.Q., Chen, Z.Q. and Ko, J.M. (2009), "Structural damage detection of cable-stayed bridges using changes in cable forces and model updating", *J. Struct. Eng. - ASCE*, **135**(9), 1093-1106.
- Jaishi, B. and Ren, W.X. (2005), "Structural finite element model updating using ambient vibration test results", *J. Struct. Eng. - ASCE*, **131**(4), 617-628.
- Kim, J., Ho, D., Nguyen, K., Hong, D., Shin, S., Yun, C. and Shinozuka, M. (2013), "System identification of a cable-stayed bridge using vibration responses measured by a wireless sensor network", *Smart Struct. Syst.*, **11**(5), 533-553.
- Ko, J.M. and Ni, Y.Q. (2005), "Technology developments in structural health monitoring of large-scale bridges", *Eng. Struct.*, **27**(12), 1715-1725.
- Ko, J.M., Ni, Y.Q. and Chan, T.H.T. (1999), "Dynamic monitoring of structural health in cable-supported bridges", *Smart Structures and Materials 1999: Smart Systems for Bridges, Structures, and Highways*, (Ed., Liu, S.C.), SPIE.
- Ko, J.M., Sun, Z.G. and Ni, Y.Q. (2002), "Multi-stage identification scheme for detecting damage in cable-stayed Kap Shui Mun Bridge", *Eng. Struct.*, **24**(7), 857-868.
- Li, Z.X., Zhou, T.Q., Chan, T.H.T. and Yu, Y. (2007), "Multi-scale numerical analysis on dynamic response and local damage in long-span bridges", *Eng. Struct.*, **29**(7), 1507-1524.
- Mufti, A.A. (2002), "Structural health monitoring of innovative Canadian civil engineering structures", *Struct. Health Monit.*, **1**(1), 89-103.
- Ni, Y.Q. and Wong, K.Y. (2012), "Integrating bridge structural health monitoring and condition-based maintenance management", *Proceedings of the 4th International Workshop on Civil Structural Health Monitoring*, Berlin, Germany (CD-ROM).
- Ni, Y.Q., Wong, K.Y. and Xia, Y. (2011), "Health checks through landmark bridges to sky-high structures", *Adv. Struct. Eng.*, **14**(1), 103-119.
- Ou, J. and Li, H. (2009), "Structural health monitoring research in China: trends and applications", *Structural Health Monitoring of Civil Infrastructure Systems*, (Eds., V.M., Karbhari. and F., Ansari), Wood head Publishing, Cambridge, UK.
- Phares, B., Lu, P., Wipf, T., Greimann, L. and Seo, J. (2013), "Field validation of a statistical-based bridge damage-detection algorithm", *J. Bridge Eng. - ASCE*, **18**(11), 1227-1238.
- Pines, D.J. and Aktan, A.E. (2002), "Status of structural health monitoring of long-span bridges in the United States", *Prog. Struct. Eng. Mater.*, **4**(4), 372-380.

- Ren, W.X., Peng, X.L. and Lin, Y.Q. (2005), "Experimental and analytical studies on dynamic characteristics of a large span cable-stayed bridge", *Eng. Struct.*, **27**(4), 535-548.
- Seo, J., B. Phares, B., Lu, P., Wipf, T. and Dahlberg, J. (2013), "Bridge rating protocol using ambient trucks through structural health monitoring system", *Eng. Struct.*, **46**, 569-580.
- Talebinejad, I., Fischer, C. and Ansari, F. (2011), "Numerical evaluation of vibration-based methods for damage assessment of cable-stayed bridges", *Comput. -Aided Civil Infrastruct. Eng.*, **26**(3), 239-251.
- Wang, H., Li, A., Hu, R. and Li, J. (2010), "Accurate stress analysis on steel box girder of long span suspension bridges based on multi-scale submodeling method", *Adv. Struct. Eng.*, **13**(4), 727-740.
- Wei, L., Cheng, H. and Li, J. (2012), "Modal analysis of a cable-stayed bridge", *Procedia Eng.*, **31**, 481-486.
- Wilson, J.C. and Gravelle, W. (1991), "Modelling of a cable-stayed bridge for dynamic analysis", *Earthq. Eng. Struct. D.*, **20**(8), 707-721.
- Wong, K.Y. (2004), "Instrumentation and health monitoring of cable-supported bridges", *Struct. Control Health Monit.*, **11**(2), 91-124.
- Wong, K.Y. and Ni, Y.Q. (2009), "Modular architecture of structural health monitoring system for cable-supported bridges", *Encyclopedia of Structural Health Monitoring*, (Eds., C., Boller, F.K., Chang and Y. Fujino), John Wiley & Sons, Chichester, UK.
- Xia, Y.X., Ni, Y.Q. and Wong, K.Y. (2013), "Development of a 3D bridge rating system incorporating structural health monitoring data", *Proceedings of the 6th International Conference on Structural Health Monitoring of Intelligent Infrastructure*, Hong Kong (CD-ROM).
- Yun, C.B., Lee, J.J. and Koo, K.Y. (2011), "Smart structure technologies for civil infrastructures in Korea: recent research and applications", *Struct. Infrastruct. E.*, **7**(9), 673-688.
- Zhang, Q.W., Chang, T.Y.P. and Chang, C.C. (2001), "Finite element model updating for the Kap Shui Mun cable-stayed bridge", *J. Bridge Eng. - ASCE*, **6**(4), 285-293.